Journal of Innovative Optical Health Sciences
Vol. 4, No. 1 (2011) 59–66

DOI: 10.1142/S1793545811001083

BINARY TISSUE CLASSIFICATION STUDIES ON RESECTED HUMAN BREAST TISSUES USING OPTICAL COHERENCE TOMOGRAPHY IMAGES

M. BHATTACHARJEE[*,‡], P. C. ASHOK[*,§], K. DIVAKAR RAO[*,†], S. K. MAJUMDER[*], Y. VERMA[*] and P. K. GUPTA[*]
[*]*Laser Biomedical Applications and Instrumentation Division*
Raja Ramanna Center for Advanced Technology
Indore 452 013, India
[†]*kdivakar@rrcat.gov.in*

We report the results of a comparative study of Fourier domain analysis (FDA) and texture analysis (TA) of optical coherence tomography (OCT) images of resected human breast tissues for binary classification between normal–abnormal classes and benign–malignant classes. With the incorporation of Fisher linear discriminant analysis (FLDA) in TA for feature extraction, the TA-based algorithm provided improved diagnostic performance as compared to the FDA-based algorithm in discriminating OCT images corresponding to breast tissues with three different pathologies. The specificity and sensitivity values obtained for normal–abnormal classification were both 100%, whereas they were 90% and 85%, respectively for benign–malignant classification.

Keywords: Optical coherence tomography; breast tissue; texture analysis; Fourier domain analysis; classification.

Optical coherence tomography (OCT) is an optical imaging technique, which can provide noninvasive, noncontact, high-resolution cross-sectional images of tissue up to a depth of 1–3 mm in near-real time.[1–3] The axial resolution of conventional OCT systems is determined by the bandwidth of the light source, and for superluminescent diode (SLD) sources normally used in the OCT devices it is $\sim 10\,\mu$m. This resolution is not sufficient to bring out the cytological differences between the normal and the abnormal tissues. However, due to the pathological processes associated with a disease, there are significant differences in the scattering properties of tissues which lead to considerable changes in the characteristic textures of the OCT images that can be exploited by various statistical techniques. For example, texture analysis (TA) of OCT images was carried out for classifying different tissue types of mouse including skin, fat, abnormal lung tissue, etc. Their success rates varied from 38% to 95% for the three categories.[4–6] Computational techniques like Fourier-domain classification and other periodicity-based algorithms have also been used in OCT images for the classification of adipose, stroma, and tumorous tissues of human breast with sensitivity and specificity values in the range of $\sim 95\%$ and $\sim 65\%$, respectively.[7] Mujat *et al.*[8] developed algorithms for automated breast tissue

[†]Corresponding author.
[‡]Presently with the Variable Energy Cyclotron Centre, Kolkata (India).
[§]Presently with the School of Physics and Astronomy, University of St. Andrews, St. Andrews, Scotland (UK).

classification based on axial scan data with sensitivity and specificity of $\sim 88\%$.[8]

In this paper, we report the results of a study of the performance of algorithms based on FDA and TA methods to differentiate the OCT images. We chose formalin-fixed resected tissues of normal human breast, fibroadenoma (FA), and invasive ductal carcinoma (IDC) tumor samples. Using the OCT images, the enhanced diagnostic ability of TA method when coupled with Fisher's linear discriminant analysis (FLDA) compared to FDA was demonstrated. Nearest mean classifier (NMC) was used for classification of the OCT images of different breast tissue types based on leave-one-out (LOO) cross-validation method.[9,10] Results show that incorporation of FLDA in texture-based algorithm makes it more accurate compared to FDA.

A schematic of the OCT setup used for the experiments is shown in Fig. 1. It comprises of an SLD of central wavelength ~ 840 nm with a bandwidth of ~ 30 nm with 5 mW optical power. The output of the SLD was coupled to a 2×2 optical fiber coupler designed to work in the range of the wavelength used. The coupler splits the light from the source to sample arm and reference arm. Light beam in the sample arm was collimated and focused to the sample using a $10\times$ objective. Light in the reference arm was collimated and coupled back into the fiber using a mirror at the reference arm.

The reference mirror was mounted on a linear translational stage scanning with a velocity of 20 mm/s, which results in a Doppler shift of 45 kHz. Light reflected from both sample arm and reference arm was coupled back to the detection arm, and the interference signal was detected with a photodiode (PD). The resulting interferogram was amplified using a transimpedance amplifier (TIA) and demodulated using a lock-in amplifier. The interferogram envelope was digitized and acquired in a PC using a data acquisition card (DAQ). Lateral scanning was done using a stepper motor. Software based on Labview was used to control the entire setup. The free space axial and lateral resolutions of the setup were estimated to be ~ 11 and $17\,\mu$m respectively.[11] The signal-to-noise ratio (SNR) of the setup was measured to be ~ 100 dB. Typical image ($1{,}000 \times 100$ pixels) acquisition time was about 1 min.

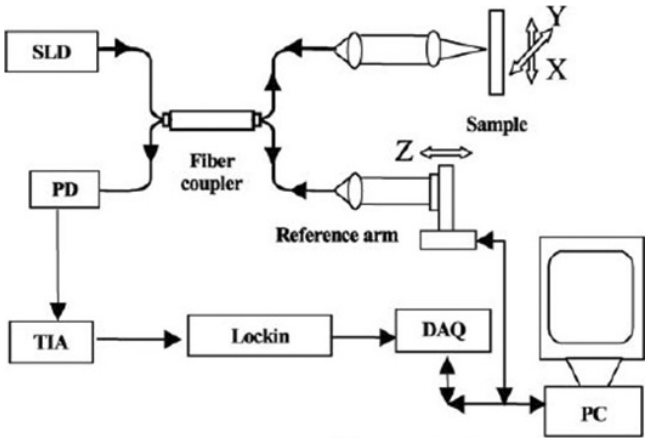

Fig. 1. Schematic view of the OCT setup used for acquiring the human breast tissue images. SLD, superluminescent diode; PD, photodiode; TIA, transimpedance amplifier; DAQ, data acquisition board.

The pathologically characterized tissue samples were obtained from the Pathology Department of CHL-Apollo Hospital, Indore following resection at surgery from patients already diagnosed of having breast tumor. For OCT measurements reported here, the tissue samples were kept preserved in formalin (10%) at room temperature (24°C). Tissue samples from only those patients were included in the study for which the histopathological diagnosis was unambiguous. The histopathological report provided by the histopathologist was taken as the "Gold Standard" for this study. The OCT images were acquired from a total of 160 sites in breast tissue samples obtained at surgery from 12 patients. The healthy tissue surrounding the breast tumor was considered "uninvolved" (normal) based on the pathologist's assessment. The typical sample size was $\sim 2\,\text{cm}^2$, and an average of 3–4 OCT images were recorded per sample.

We used FDA and TA methods to carry out the feature extraction and tissue classification of the OCT image dataset. Figure 2 gives the flowchart of the sequence followed in the study. Binary classification of two types were attempted: IDC-FA (benign–malignant) classification and normal–abnormal classification where both IDC and FA were together categorized as abnormal. For both these methods, the evaluation was carried out by LOO cross-validation method.[10,12] It involved using a single dataset from the original dataset as the validation data and the remaining observations as the training data and repeating the same for all the datasets. Finally, the confusion matrices were generated for quantifying the diagnostic ability of each of the methods.

Typical images recorded in this study correspond to a size of 2 mm (depth) and 3 mm (lateral). The

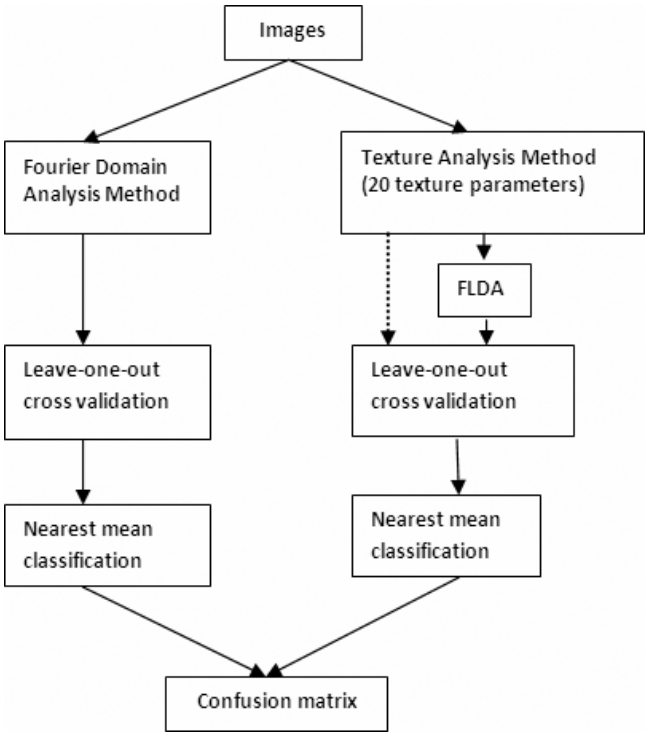

Fig. 2. Flowchart of the processing steps. FLDA — Fisher linear discriminant analysis.

raw image was recorded in 12 bits to a matrix of size 150 (lateral) × 1,000 (depth) which was then resized to 400×600 pixels using bicubic interpolation for maintaining the optimum aspect ratio. The upsampling in the transverse dimension did not lead to significant changes in the diagnostic results as the pixel size is comparable to the lateral resolution. Image preprocessing was carried out for noise suppression using thresholding and masking. Threshold intensity level was determined by the random fluctuation of intensity in the region above the tissue sample in the OCT image. Using edge detection technique, air tissue interface was determined and the region above the interface was masked during the analysis. The region below 750 μm was also masked during the analysis as there was no morphological information below this depth.

The basic principle of FDA-based image classification is that the spatial frequency component in axial scans (A-scans) of the tissue depends on the characteristic periodic structure of the tissue. The Fourier power spectrum is expected to have dominant small frequency for adipose tissue due to the large cellular structure compared to the benign or malignant tumor tissues where the Fourier spectrum is expected to have broad features. The variation in the spatial frequencies for different types of tissues can be exploited for automated tissue classification.

To perform FDA-based classification, a set of histologically categorized breast tissue sample images were used as the input, and this formed the training set. For each image, 512-point FFT was evaluated for each of its A-scan and the average of the FFT spectrum was evaluated. The next step was the classification of the images based on the FFT spectrum using LOO method. Each FFT vector was taken out as the validation data $Q(k)$, and the average Fourier spatial spectrum ($R_{\text{tissue}}(k)$) was evaluated for all the three categories excluding the dataset $Q(k)$. $Q(k)$ was classified with respect to the corresponding training set of data using nearest mean distance classifier that involved minimizing the quantity MD_{tissue} in Eq. (1) below. The classification results obtained thus were saved in a confusion matrix.

$$MD_{\text{tissue}} = |Q(k) - R(k)|^2. \tag{1}$$

"Texture" is a general term used for quantifying properties like smoothness, coarseness, regularity, etc., of a surface. Technically, image texture is defined as a function of the spatial variation in pixel intensities (gray values). Statistical TA techniques exploit this correlation between different pixel intensity values and use them for computing certain statistical parameters which ultimately characterize the texture of the image.

In our study, we used the spatial gray-level dependence matrix (SGLDM)-based statistical texture analysis for the classification of OCT images of breast tissues. SGLDM which is also termed as gray-level co-occurrence matrix (GLCM) is produced from an image by calculating how often a pixel with the intensity (gray-level) value i occurs in a specific spatial relationship to a pixel with the value j.[13,14] The parameter termed "distance" determines the distance between the pixels, whose spatial relationship is to be estimated, and "angle" specifies the direction in which one pixel lies with respect to the other. If the image is composed of L gray-levels, then the GLCM is an LXL matrix, each element of which is the probability, $s_\theta(i, j/d)$ of the pixel with gray-level value i being "d" distance away from the pixel with gray-level value j in a certain angle θ. The GLCM was evaluated for four possible orientation angles between pixels i and j, namely, 0°, 45°, 90°, and 135° and five different statistical parameters were evaluated from the

matrices. The images used for this analysis were downsampled to eight levels from 256 gray-levels. The optimized value of pixel distance "d" was estimated to be 6 pixels in the rescaled images so that the distinctive texture information in the OCT images of each category of tissues could be extracted for efficient classification.

The five statistical parameters with their mathematical and physical significance are described in Table 1.[5,13] Here, μ_x and μ_y are the means of rows and columns of GLCM, respectively and σ_x and σ_y are the corresponding standard deviations. The five parameters evaluated in four directions formed a 20-dimensional feature vector for each image. Using LOO cross-validation, each image in the dataset was classified into the corresponding category keeping rest of the dataset as the training dataset and by using NMC approach. The results thus obtained were saved in a confusion matrix.

The efficacy of the TA-based classification was tested in one-dimensional space using FLDA method used for dimensionality reduction of feature space.[15,16] If c is the number of classes, then FLDA reduces the dimensionality to $c-1$ in such a way that maximum intraclass mean distance is minimized and the interclass mean distance is maximized. This defines Fisher's criterion which is maximized over all linear projections (w):

$$J(w) = \frac{|\mu_1 - \mu_2|^2}{S_1^2 + S_2^2}. \tag{2}$$

Here, μ represents the mean, S^2 represents the variance, and the subscripts denote the two classes. Maximizing this criterion yields a closed-form solution that involves the inverse of a covariance-like matrix. The time to optimize the parameters of an algorithm over a training set data depends on its size and dimensionality and can vary from few seconds to even several minutes. In contrast, the time taken to classify an unseen image will always be a matter of few seconds. Since the size and dimension of the training set data in our case were 160 and 20, respectively, the time taken for both training and validating our algorithm took only several seconds.

Figure 3 shows the OCT images of normal, benign, and malignant breast tissue samples recorded with the setup shown in Fig. 1. Significant differences in the texture of scattering pattern for different types of breast tissue samples are apparent. Cell structure of normal fatty (adipose) tissue is seen to be well resolvable. Since the adipose tissues are composed of cells (85% of which is filled with lipid droplet and the rest 15% with a layer of cytoplasm surrounding it) larger in diameter ($\sim 100\,\mu$m) with comparatively lesser structures, they can be well resolved in a conventional OCT system.[4] On the other hand, the FA and IDC samples have relatively higher scattering primarily due to increased regional cell density. As the neoplastic transformation in the tissue changes the tissue architecture increasing the cell density, enhanced scattering is seen in both malignant and benign tissues. The attenuation was relatively less for normal tissues, and distributed scattering regions were visible. In contrast to the low-scattering regions of adipocytes of normal tissue, the benign and malignant samples, due to the solid tumor, showed relatively dense and smooth scattering with the scattering intensity slightly higher for malignant tissues as compared to the benign ones.[17]

Table 1. The five statistical texture parameters evaluated from GLCM.

Statistical parameters	Physical significance	Mathematical description
Contrast	Measures the local variations in the GLCM.	$\sum_{i=0}^{L-1}\sum_{j=0}^{L-1}(i-j)^2 s_\theta(i,j\,\vert\,d)$
Energy	Sum of squared elements in the GLCM. Also known as uniformity or the angular second moment.	$\sum_{i=0}^{L-1}\sum_{j=0}^{L-1}[s_\theta(i,j\,\vert\,d)]^2$
Correlation	Measures the joint probability occurrence of the specified pixel pairs.	$\frac{\sum_{i=0}^{L-1}\sum_{j=0}^{L-1}(i-\mu_x)(j-\mu_y)s_\theta(i,j\,\vert\,d)}{\sigma_x\sigma_y}$
Entropy	Measures the randomness of values of elements in GLCM.	$\sum_{i=0}^{L-1}\sum_{j=0}^{L-1} s_\theta(i,j\,\vert\,d)\log[s_\theta(i,j\,\vert\,d)]$
Homogeneity	Measures the closeness of the distribution of elements in the GLCM to the GLCM diagonal.	$\sum_{i=0}^{L-1}\sum_{j=0}^{L-1}\frac{1}{1+(i-j)^2}s_\theta(i,j\,\vert\,d)$

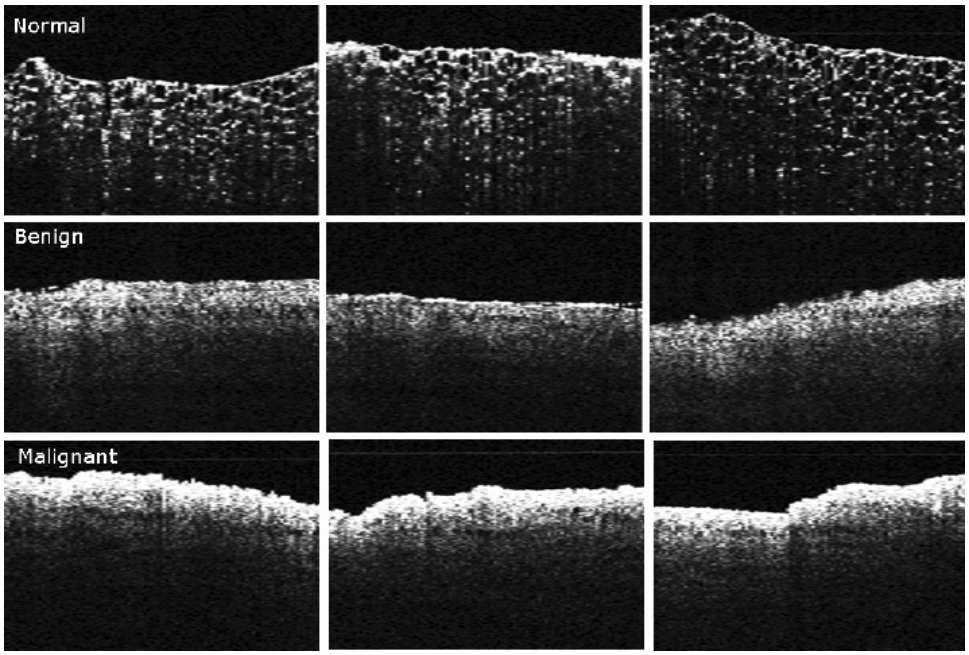

Fig. 3. OCT images of normal (1st row), benign (2nd row), and malignant (3rd row) human breast tissue samples. Normal tissues show cellular structures due to large lipid-filled cells, whereas benign and malignant show uniform scattering. (Depth × Lateral — 2 mm × 3 mm for each image.)

Since the scattering properties of the benign and malignant ones were similar, their classification was the most challenging task in this study.

The texture analysis code used in the study was validated using Brodatz textures.[4] The probability of correct classification rates of these standard textures in our case ranged from 80% to 100% which gave us confidence about the reliability of the code we were using. Two types of classification were attempted, FA−IDC (benign−malignant) and normal−abnormal classification with FA and IDC together categorized as abnormal using LOO cross-validation method. Tables 2(a) and 2(b) summarize the results obtained for these two types of classification and compares the efficacy of FDA, TA, and also FLDA-incorporated TA (TA−FLDA) method for each type individually.

The confusion matrix for each type of classification has been tabulated above. As can be observed, while abnormal (benign + malignant) tissues could

Table 2(a). Normal−abnormal classification.

	FDA (%)		TA (%)		TA−FLDA (%)	
Histopathology	Normal	Abnormal	Normal	Abnormal	Normal	Abnormal
Normal	100	0	70	30	100	0
Abnormal	17.19	82.81	17.97	82.03	0	100

Table 2(b). Benign−malignant classification.

	FDA (%)		TA (%)		TA−FLDA (%)	
Histopathology	Benign	Malignant	Benign	Malignant	Benign	Malignant
Benign	68	32	60.5	39.5	90	10
Malignant	29.8	70.2	59.5	40.5	15	85

be distinguished from normal tissues with very good confidence level (specificity and sensitivity of 100%), the classification results for distinguishing benign tissues from malignant ones were not that satisfactory. This is to be expected since the scattering properties of the normal sites were visually distinguishable from the benign and the malignant sites. Both the TA and the FDA method failed to yield satisfactory classification results for this type, the maximum specificity and sensitivity obtained being in the range of $\sim 70\%$, as shown in Table 2(b). Finally, with the incorporation of FLDA in TA, the specificity and sensitivity reached up to a satisfactory level of 90% and 85%, respectively. This enhanced performance with the incorporation of FLDA is due to the fact that FLDA projects data in a line that would preserve the direction useful for data classification. In other words, it reduces the dimensionality of the dataset while preserving as much of the discriminatory information as possible.

The relative performance of the different diagnostic algorithms was assessed by carrying out a receiver-operating characteristic (ROC) analysis of the corresponding classification results.[18–20] An ROC curve provides a visual comparison of the tradeoff between sensitivity and specificity of a diagnostic test. The ROC curve was generated for each diagnostic algorithm with respective validation dataset by plotting the true positive rate (sensitivity) as a function of the false positive rate (1-specificity) as the classification threshold was varied. Area under the ROC space is taken as a quantitative measure of the performance of the algorithm. The closer the area is to 1, the more accurate is the corresponding diagnostic algorithm.

Figures 4(a) and 4(b) show the ROC curves for both types of classification. The diagnostic performance of FDA method was observed to be superior compared to the TA method. However, incorporation of FLDA in TA improved the corresponding AOC close to 1 almost to the idealistic limit for normal–abnormal and close to 90% in case of benign–malignant classification. The relative performances of the algorithms degraded from TA–FLDA to FDA followed by TA for both types of classifications.

FDA analysis of the different breast tissues showed that the low-frequency components in the Fourier spectra of normal tissues are more as compared to that for benign or malignant samples. This is in qualitative agreement with the studies reported

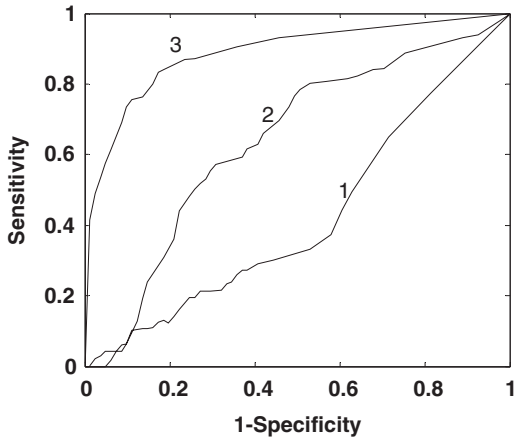

(a)

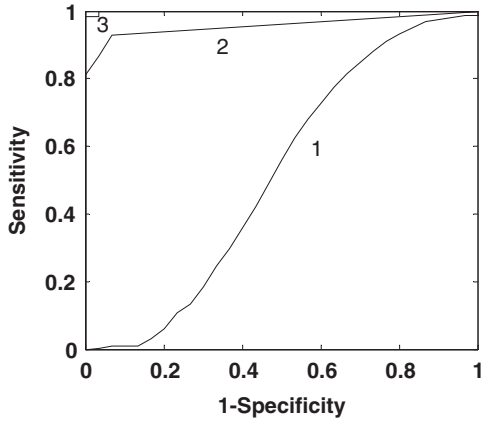

(b)

Fig. 4. (a) ROC curve for (1) TA, (2) FDA, and (3) TA–FLDA methods for benign–malignant classification. (b) ROC curve for (1) TA, (2) FDA, and (3) TA–FLDA methods for normal–abnormal tissue classification.

by Zysk and Boppart[7] who used fresh tissues for imaging. In our case, the Fourier power spectrum of the normal tissues dominates over that of the malignant ones up to a spatial frequency value of $2 \times 10^4\,\mathrm{m}^{-1}$ and after that the trend reverses. The cutoff value in our case was at $\sim 4 \times 10^4\,\mathrm{m}^{-1}$ that is in close agreement with the results of Zysk and Boppart.[7] TA was shown to give high classification rates for tissue phantoms[6] and different tissue types such as mouse fat versus mouse skin.[4] Iftimia *et al.*[21] used mean values of several parameters of OCT axial scans such as signal slope, variance, power spectrum, mean spatial frequency, etc., to differentiate the breast tissue types with a fine needle probe and obtained $\sim 93\%$ accuracy in differentiating fatty tissue from fibrous or tumor tissue.

The results obtained in the present study demonstrate that OCT could be developed as a concurrent diagnostic tool to standard histopathological procedures for clinical diagnosis of formalin-fixed tissue specimens.[22] In a recent study, Nguyen *et al.*[23] demonstrated potential of intraoperative real-time OCT for detection of surgical boundaries of breast tissues in operating room with 100% sensitivity and 82% specificity. Although we also achieved 100% sensitivity and specificity in separating OCT images of normal from abnormal breast tissues, it is important to mention here that the normal breast tissue samples used in our study were adipose tissues with large amount of fat covering the underlying fibrous and glandular tissues. Although due to limited sample size we have not included the fibrous/glandular tissues in the normal category for validating our diagnostic algorithm, results of recent studies have demonstrated that OCT can successfully delineate breast tumors from normal fibrous/glandular tissues as well.[21,23] Further, it is pertinent to mention that although in the present study we have developed classification algorithms to discriminate OCT images of different breast tissue types, the algorithms can be used for discriminating tissue types in other organ systems as well. For example, it has been shown that algorithms based on texture analysis can be used to identify lung and skin tissues.[4] The framework of the algorithm can be easily extended for analyzing the diagnostic content of the OCT images from fresh breast tissues as well.

It is pertinent to note that we have not employed any feature selection method as part of the development of the present discrimination algorithm. This is because, it is not known *a priori* which subset of features are relevant for a given classification problem. The selection of an optimal subset of features from a set of features is always an optimization problem and is often facilitated by use of a performance measure for each subset of features to measure their ability to classify the samples. Attempting a brute-force search of the best combination of features (combination of 2, 3, or more number of features of the whole set of features) is impractical, because the number of possible feature combinations can be prohibitively large for the set of features with a high dimension. One widely used approach is to rank the features based on some feature ranking criteria designed to evaluate how well an individual feature contributes to the separation (e.g., cancer vs. normal) and then use a fixed number of top ranked features as input to the classifier. This method has the important drawback in that if some of the features (say the least ranked) are eliminated and feature ranking is repeated, then the rank of the remaining features changes from the previous values. Therefore, use of this approach to generate optimal subset of features is debatable. Moreover, the performance of FLDA is expected not to be affected whether one does feature selection prior to using FLDA.

In summary, we have carried out a comparative study of FDA and TA for identification of three different histological tissue types of human breast tissues. In the Fourier analysis method, the variation in spatial frequency component of A-scans in images of each category was evaluated for tissue classification while various statistical texture parameters were evaluated in the latter to extract the information about the local repetitive structures in the images due to speckle. The results of the computational analysis of OCT images from normal, benign, and malignant sites show that due to the morphological differences in the tissue sites, the success rates of classification also vary depending on the pair of validation dataset. The normal tissue sites could be easily distinguished from the abnormal (benign/malignant) sites with very high value of specificity and sensitivity. However, distinguishing benign from malignant sites is a more difficult prospective. Comparative study on the use of FDA and TA showed that use of TA−FLDA hybrid algorithm improves the efficiency of the TA method. The TA−FLDA combined algorithm proved successful in increasing the accuracy of benign−malignant classification as compared to either TA or FDA alone.

References

1. A. F. Fercher, W. Drexler, C. K. Hitzenberger, T. Lasser, "Optical coherence tomography — Principles and applications," *Rep. Prog. Phys.* **66**, 239−303 (2003).
2. A. Gh. Podoleanu, "Optical coherence tomography," *Br. J. Radiol.* **78**, 976−988 (2005).
3. K. D. Rao, A. Alex, Y. Verma, S. Thampi, P. K. Gupta, "Real-time *in vivo* imaging of adult Zebrafish brain using optical coherence tomography," *J. Biophotonics* **2**, 288−291 (2009).
4. K. W. Gossage, T. Tkaczyk, J. Rodriguez, J. K. Barton, "Texture analysis of optical coherence tomography images: Feasibility for tissue classification," *J. Biomed. Opt.* **8**, 570−575 (2003).

5. S. A. Boppart, W. Luo, D. L. Marks, K. W. Singletary, "Optical coherence tomography: Feasibility for basic research and image-guided surgery of breast cancer," *Breast Cancer Res. Treat.* **84**, 85−97 (2004).
6. K. W. Gossage, C. M. Smith, E. M. Kanter, L. P. Hariri, A. L. Stone, J. J. Rodriguez, S. K. Williams, J. K. Barton, "Texture analysis of speckle in optical coherence tomography images of tissue phantoms," *Phys. Med. Biol.* **51**, 1563−1575 (2006).
7. A. M. Zysk, S. A. Boppart, "Computational methods for analysis of human breast tumor tissue in optical coherence tomography images," *J. Biomed. Opt.* **11**, 054015 (2006).
8. M. Mujat, D. R. Ferguson, D. X. Hammer, C. Gittins, M. Iftimia, "Automated algorithm for breast tissue differentiation in optical coherence tomography," *J. Biomed. Opt.* **14**, 034040 (2009).
9. A. Luntz, V. Brailovsky, "On estimation of characters obtained in statistical procedure of recognition (in Russian)," *Techicheskaya Kibernetica* **3**, (1969).
10. G. C. Cawley, N. L. C. Talbot, "Efficient leave-one-out cross validation of kernel Fisher discriminant classifiers," *Pattern Recogn.* **36**, 2585−2592 (2003).
11. Y. Verma, K. D. Rao, M. K. Suresh, H. S. Patel, P. K. Gupta, "Measurement of gradient refractive index profile of crystalline lens of fisheye *in vivo* using optical coherence tomography," *Appl. Phys. B* **87**, 607−610 (2007).
12. B. D. Goldberg, N. V. Iftimia, J. E. Bressner, M. B. Pitman, E. Halpern, B. E. Bouma, G. J. Tearney, "Automated algorithm for differentiation of human breast tissue using low coherence interferometry for fine needle aspiration biopsy guidance," *J. Biomed. Opt.* **13**, 014014 (2008).
13. R. M. Haralick, K. Shanmugam, I. Dinstein, "Texture features for image classification," *IEEE Trans. Syst. Man Cybern.* SMC **3**, 610−621 (1973).
14. F. Argenti, L. Alparone, G. Benelli, "Fast algorithms for texture analysis using co-occurrence matrices," *IEEE Proc., Pt. F* **137**, 443−448 (1990).
15. B. Liefeng, L. Wang, L. Jiao, "Feature scaling for kernel Fisher discriminant analysis using leave-one-out cross validation," *Neural Comput.* **18**, 961−978 (2006).
16. S. Mika, G. Ratsch, J. Weston, B. Scholkopf, K. R. Mullers, "Fisher discriminant analysis with kernels," *IEEE Signal Proc. Soc.*, Workshop Berlin (1999).
17. P. L. Hsiung, D. R. Phatak, Y. Chen, A. D. Aguirre, J. G. Fujimoto, J. L. Connolly, "Benign and malignant lesions in the human breast depicted with ultrahigh resolution and three-dimensional optical coherence tomography," *Radiology* **244**, 865−874 (2007).
18. S. K. Majumder, N. Ghosh, P. K. Gupta, "Support vector machine for optical diagnosis of cancer," *J. Biomed. Opt.* **10**, 024034 (2005).
19. S. K. Majumder, N. Ghosh, P. K. Gupta, "Relevance vector machine for optical diagnosis of cancer," *Lasers Surg. Med.* **36**, 323−333 (2005).
20. J. A. Hanley, B. J. McNeil, "The meaning and use of the area under a receiver operating characteristic (ROC) curve," *Radiology* **143**, 29−36 (1982).
21. N. V. Iftimia, M. Mujat, T. Ustun, R. D. Ferguson, V. Danthu, D. X. Hammer, "Spectral-domain low coherence interferometry/optical coherence tomography system for fine needle breast biopsy guidance," *Rev. Sci. Instrum.* **80**, 024302 (2009).
22. P. L. Hsiung, P. R. Nambiar, J. G. Fujimoto, "Effect of tissue preservation on imaging using ultrahigh resolution optical coherence tomography," *J. Biomed. Opt.* **10**, 064033 (2005).
23. F. T. Nguyen, A. M. Zysk, E. J. Chaney, J. G. Kotynek, U. J. Oliphant, F. J. Bellafiore, K. M. Rowland, P. A. Johnson, S. A. Boppart, "Intraoperative evaluation of breast tumor margins with optical coherence tomography," *Cancer Res.* **69**, 8790−8796 (2009).